Ocean Sci. Discuss., 11, 1561–1611, 2014
www.ocean-sci-discuss.net/11/1561/2014/
doi:10.5194/osd-11-1561-2014

Ocean Science
Discussions
Open Access

Modelling survival and connectivity of *Mnemiopsis leidyi* in the southern North Sea and Scheldt estuaries

J. van der Molen[1], J. van Beek[2], S. Augustine[6], L. Vansteenbrugge[4,5], L. van Walraven[3], V. Langenberg[2], H. W. van der Veer[3], K. Hostens[4], S. Pitois[1], and J. Robbens[4]

[1]The Centre for Environment, Fisheries and Aquaculture Science (CEFAS), Lowestoft, UK
[2]Deltares, Delft, the Netherlands
[3]Royal Netherlands Institute for Sea Research (NIOZ), Den Burg (Texel), the Netherlands
[4]Institute for Agricultural and Fisheries Research (ILVO), Oostende, Belgium
[5]Biology Department, Faculty of Sciences, Ghent University (UGent), Gent, Belgium
[6]Center for Ocean Life, Charlottenlund, Denmark

Received: 30 May 2014 – Accepted: 3 June 2014 – Published: 20 June 2014

Correspondence to: J. van der Molen (johan.vandermolen@cefas.co.uk)

Published by Copernicus Publications on behalf of the European Geosciences Union.

Abstract

Three different models were applied to study the reproduction, survival and dispersal of *Mnemiopsis leidyi* in the Scheldt estuaries and the southern North Sea: a high-resolution particle tracking model with passive particles, a low resolution particle tracking model with a reproduction model coupled to a biogeochemical model, and a dynamic energy budget (DEB) model. The results of the models, each with its strengths and weaknesses, suggest the following conceptual situation: (i) the estuaries possess enough retention capability to keep an overwintering population, and enough exchange with coastal waters of the North Sea to seed offshore populations; (ii) *M. leidyi* can survive in the North Sea, and be transported over considerable distances, thus facilitating connectivity between coastal embayments; (iii) under current climatic conditions, *M. leidyi* may not be able to reproduce in large numbers in coastal and offshore waters of the North Sea, but this may change with global warming – however this result is subject to substantial uncertainty. Further quantitative observational work is needed on the effects of temperature, salinity and food availability on reproduction and on mortality at different life stages to improve models such as used here.

1 Introduction

1.1 Background

The ctenophore *Mnemiopsis leidyi* originates from tropical to warmer temperate waters along the East coast of the American continent (Boersma et al., 2007; Gesamp, 1997; Lehtiniemi et al., 2012; Purcell et al., 2001). *Mnemiopsis leidyi* is notorious for its highly adaptive life traits. A fast growth rate combined with high fecundity, early reproduction, the ability of self-fertilization and a euryoecious lifestyle tolerating a wide range of environmental parameters (temperature, salinity, water quality) are characteristics which favor its establishment and fast expansion in invaded areas (Purcell et al., 2001; Fuentes

OSD
11, 1561–1611, 2014

et al., 2010; Jaspers et al., 2011; Salihoglu et al., 2011). *Mnemiopsis leidyi* larvae and adults feed on a wide range of micro- and macro-zooplankton (Purcell et al., 2001; Sullivan and Gifford, 2004, 2007).

In the 1980s *M. leidyi* was introduced in the Black Sea, probably through ballast water (Vinogradov et al., 1989). The presence of *M. leidyi* together with eutrophication and overfishing caused a deterioration of the ecosystem, which finally degraded to a low biodiversity "dead-end" gelatinous food web (Shiganova, 1998). This led to an economic loss/collapse of the pelagic fish population, in particular anchovies and sprat fisheries (Kideys, 2002). *M. leidyi* spread further to the Caspian Sea in 1999 (Ivanov et al., 2000), to the Mediterranean Sea in 2009 (Fuentes et al., 2010) and further on into European Atlantic coastal waters. It has been observed in Le Havre Harbour since 2005 (Antajan et al., 2014). In 2007, the species was found in Belgian waters in the harbour of Zeebrugge (Dumoulin, 2007; Vanginderdeuren et al., 2012) and since 2009 it has also been observed frequently along the French coast of the North Sea (Antajan et al., 2014).

The North Sea is the home of commercially important fish stocks and spawning and nursery grounds (Ellis et al., 2011), and also shares the depleted state of fish stocks that characterized the Black Sea when *M. Leidyi* was introduced (Boersma et al., 2007; Fuentes et al., 2010). Furthermore, recent work from Collingridge et al. (2014) found that large parts of the North Sea were suitable for *M. leidyi* reproduction in summer months, with some of the highest risk areas along the southern coastal and estuarine regions of the North Sea, due to a combination of high temperatures and high food concentrations. The presence and potential establishment of *M. leidyi* in the southern North Sea is therefore cause for concern, and there is a need to further our understanding on the mechanisms involved in the dynamics of *M. leidyi* populations and its potential spread from source locations where it is established.

In this paper we apply three different models to simulate aspects of transport and reproduction of *M. leidyi* in the Scheldt estuaries and the North Sea. We use the combined results to provide insight into the potential spreading and population dynamics of

OSD
11, 1561–1611, 2014

M. leidyi at a range of spatial and temporal scales in the area that could not have been obtained with each model individually.

1.2 Study area

1.2.1 Scheldt estuaries

The Western Scheldt is the Dutch part of the estuary of the Scheldt River which flows from France to Belgium and enters the North Sea in the Netherlands, see Fig. 1. The total surface area of the Western Scheldt is approximately 310 km^2 and it has a length of about 60 km. The average channel depth is 15–20 m (Meire et al., 2005) and the estuary has extensive tidal flats. The Scheldt River has an average fresh-water discharge of 104 $m^3 s^{-1}$ and the upstream part in Belgium has the characteristics of a tidal river. The salinity at the Belgian–Dutch border ranges from 2 to 14 PSU and the maximum tidal range is 5 m. The Scheldt is considered well mixed, except in periods of peak river discharge (Meire et al., 2005).

The Eastern Scheldt estuary is the former mouth of the Scheldt river and has a connection to the Rhine and Meuse river system, see Fig. 1. The total surface area of the Eastern Scheldt is approximately 350 km^2 and it has a length of about 40 km. The inner part of the Estuary is forked, with a smaller branch to the north and a wider branch to the south east. Following the 1953 storm surge, waterworks have been constructed which isolate the Eastern Scheldt from most of the fresh water input, transforming the estuary into a well-mixed tidal bay. In the mouth of the estuary a storm surge barrier has been constructed which is usually open, but can be closed under extreme weather conditions. The barrier reduces the exchange of water with the open sea by 28 % (Smaal and Nienhuis, 1992).

The two estuaries are only connected by sluiced waterways. Both estuaries have a protected status as nature reserve.

OSD
11, 1561–1611, 2014

1.2.2 Southern North Sea

The southern North Sea is a relatively shallow shelf sea with depths less than 80 m. The most prominent feature is the Dogger Bank, which rises up to less than 30 m water depth, and is separated from the Norfolk Banks to the southwest by the Silver Pit. The latter has a depth of over 50 m. To the southeast of the Dogger Bank are the Oyster Grounds, with depths of 40–50 m. The Southern Bight is situated further south, and consists of a deep channel (depth up to 50 m) in the west and a shallow area (depths typically less than 30 m) in the east. The channel is connected to the Strait of Dover to the south.

The tides in the southern North Sea are semi-diurnal, with dominant M_2 tidal amplitudes over 2 m along the UK east coast, near Dover Strait, and in the German Bight, and amphidromic points in the central southern North Sea and in the Southern Bight of the North Sea (e.g., Davies et al., 1997). Maximum surface currents at spring tide are about 1.4 m s^{-1} in the western and southern parts of the Southern Bight, reducing to 0.3 m s^{-1} in the central southern North Sea (Hydrographical Survey, 2000).

Wind can induce depth-averaged surge currents of up to 1 m s^{-1} (Flather, 1987). The time and depth-averaged atmospherically-induced residual currents are about 1/3 of the tidal residuals and directed to the north in the Southern Bight, and to the northeast in the southern North Sea (Prandle, 1978). Combined residual current speeds in the Southern Bight are approximately 0.05 m s^{-1} (Prandle, 1978).

Thermal stratification occurs in summer in the northern parts of the southern North Sea, whereas the southern parts remain well-mixed, and are separated by the Frysian Front (Otto et al., 1990). Under stratified conditions, a subsurface jet induced by density differences transports water around the north, east and southeast slopes of the Dogger Bank into the Oyster Grounds (Brown et al., 1999; Hill et al., 2008). The thermal stratification breaks down in the autumn, and is absent throughout the winter.

On a more local scale, fresh-water outflow of the river Rhine forms a plume along the Dutch coast to the North, resulting in density-driven coastward near-bottom currents of

OSD
11, 1561–1611, 2014

several cm s^{-1} (Visser, 1992). A similar plume is present in the German Bight and associated with the river Elbe (e.g. Schrum, 1997). UK coastal waters converge in the East Anglian plume, which is mostly recognisable by its elevated levels of turbidity. This plume crosses the North Sea in a northeast-ward direction, from the coast of East Anglia to the south of the Dogger Bank (see Dyer and Moffat, 1998 for a detailed description).

1.3 Multi-model approach

Three existing models were used (Delft 3D, GETM-ERSEM-BFM model with particle tracking (GITM) and the Dynamic Energy Budget (DEB) model), with limited adaptations, to simulate aspects of transport and reproduction of *M. leidyi* in the Scheldt estuaries and the North Sea. Through intercomparison of the results, and by deploying the strengths of the individual models, the combined results provide insight into the potential spreading and population dynamics of *M. leidyi* at a range of spatial and temporal scales in the area that could not have been obtained with each model individually, and without the investment required to develop a single model to encompass all. The Delft3D model implementation at high spatial resolution in the estuaries, and with tracking of passive particles provided insight into the potential role of the Scheldt estuaries as a nursery and source of *M. leidyi*, and in the role of estuarine-marine exchange processes. The GETM-ERSEM-BFM model with particle tracking (GITM) was developed to include a simple reproduction model, and was used to study transport, connectivity and population dynamics at the scale of the North Sea. The DEB model was then used to simulate in greater detail how temperature and food concentrations dynamically affect the eco-physiology of a growing, developing and/or reproducing individual. In this model age and size at important life-history events can (dramatically) depend on the prior temperature and food experienced by the individual. The DEB model was used to both gain confidence in the simple reproduction model in GITM and to expose its limitations.

OSD
11, 1561–1611, 2014

2 Material and methods

2.1 Delft3D

2.1.1 Hydrodynamics

Delft3D is an integrated modelling suite used to simulate three-dimensional flow, sediment transport and morphology, waves, water quality and ecology and the interactions between these processes. More specifically, the hydrodynamic module simulates non-steady flows in relatively shallow water, and incorporates the effects of tides, winds, air pressure, density differences (due to salinity and temperature), waves, turbulence and drying and flooding (Lesser et al., 2004).

The model application of the southern North Sea uses a curvilinear boundary fitted c-grid. The domain decomposition technique creates extra resolution by inserting an intermediate and a fine sized domain near the Dutch coast (Fig. 2). The horizontal resolution ranges from 0.5 km near the coast to 25 km near the open boundaries, resulting in 22 473 active computational elements. The vertical dimension consists of 12 σ transformed layers with the highest resolution near the sea bed and the sea surface. The shallow-water hydrostatic pressure equations are time-integrated by means of an alternating direction implicit (ADI) numerical scheme in horizontal directions and by the Crank–Nicolson method in the vertical direction. The solution is mass-conserving at every grid cell and time step. This code is extended with transport of salt and heat content and with a k-ε turbulence model for vertical exchange of horizontal momentum and matter or heat. Along the open sea boundaries tidal harmonics for water level are imposed consisting of 50 astronomical constituents. The model was forced using meteorological data from the High Resolution Limited Area Model (HIRLAM) run at the Royal Dutch Meteorological Service (KNMI) (Undén et al., 2002): two horizontal wind velocity components, air pressure and temperature, archived every 6 h. The freshwater discharges from 18 rivers were included in the model. Seven of these discharges

OSD
11, 1561–1611, 2014

varied temporally (historic daily averages) and 11 were constant (based on long-term averages).

The primary focus of the hydrodynamic model is the representation of the water level and tidal flow velocities along the Dutch coast and in the estuaries. The results of the model have been applied and validated against observational data in the modelling of suspended matter (van Kessel et al., 2011), eutrophication (Los et al., 2008) and the transport of fish larvae (Bolle et al., 2009; Dickey-Collas et al., 2009).

2.1.2 Particle tracking

The particle module uses a numerical advection scheme for particles that is fully compatible with the local mass conserving advection properties of the underlying flow field at the discrete level of that field (Postma et al., 2013). Horizontal dispersion is accounted for by a random walk step. The depth varying vertical diffusion as calculated by the hydrodynamic turbulence model is incorporated by a stochastic bouncing-algorithm which closely approximates the analytical solution.

The particle tracking module is run offline, for this purpose the hydrodynamic results are stored on an hourly basis. The particle model itself runs with a timestep of 5 min.

For the simulation of biological vectors a module is available to simulate development and vertical migration behaviour. The development is divided into an unlimited amount of stages where the duration of the stage is dependent on the age of the particle and the accumulated temperature encountered over that stage (Bolle et al., 2009). For each stage the behaviour can be set with its own parameterisation. Apart from neutral buoyancy the types of behaviour are positive buoyancy, negative buoyancy, diurnal vertical migration, selective tidal transport and settling towards the sea bed. Growth and mortality based on food availability and predation were not incorporated in the model.

OSD
11, 1561–1611, 2014

2.1.3 Application: estuaries

The Delft3D model was applied to determine the potential connectivity of *M. leidyi* between the Eastern and Western Scheldt estuaries and the North Sea. Applying the hydrodynamic situation from 2008, a run with a uniform initial distribution of particles over the estuary volume (particles m^{-3}) was performed for each estuary and for each month of the year. The boundaries of the estuaries are shown in Fig. 1. Five hundred thousand particles were released simultaneously. The horizontal dispersion coefficient was set to 1.0 ($m^2\ s^{-1}$) and no behaviour was included.

The simulations were performed from the first high tide of the month to the first high tide after a period of 30 days, which corresponds with two spring neap cycles. At the end of the simulation the position of the particles within six pre-defined areas was scored and reported as a percentage of the number of particles released, resulting in a connectivity matrix. The areas were the Eastern Scheldt estuary, the Western Scheldt estuary, the Eastern Scheldt ebb-tidal delta, Western Scheldt ebb-tidal delta, the Zeebrugge harbour area and the remainder of the North Sea as far as covered by the outer model domain (Fig. 1).

In addition to the simulations described above, model runs were carried out with initial conditions based on observations. These initial conditions were constructed using zero order extrapolation of the measurements in the lateral direction of the estuary and interpolation in the longitudinal direction with a zero value outside the estuary. Model runs were carried out from the date of measurements until the next set of measurements available for comparison.

For the Western Scheldt the model was run from 1 September 2011 to 1 December 2011. The initial field was based on samples collected in the Western Scheldt onboard R/V *Zeeleeuw* at three different locations using a WP3 net (Ø 1 m, mesh size 1 mm) in oblique hauls. Ctenophores, among which *M. leidyi*, were isolated from the samples and morphologically identified, counted and measured (oral-aboral length) on board (Vansteenbrugge et al., 2014).

OSD
11, 1561–1611, 2014

For the Eastern Scheldt the initial condition was constructed from measurements on 28 September 2012 (Van Walraven et al., 2014) onboard R/V *Luctor* using the same gear and method. The model was compared with data from the MEMO cruise on 20 October 2012 (include reference MEMO cruise lead by France). The model was run with 2011 hydrodynamics for the same period because a hydrodynamics simulation for 2012 was not available.

2.2 Particle tracking IBM coupled to GETM-ERSEM-BFM

2.2.1 Particle tracking IBM (GITM)

The Individual Behaviour Model (IBM) GITM (General Individuals Transport Model) includes physical particle advection and diffusion, and biological development and behaviour. The advection–diffusion elements of GITM were based on a re-coded version of the lagrangean semi-analytical advection–diffusion method developed by Wolk (2003). This method ensures that particles follow stream lines exactly. Furthermore, a random walk method with advective correction (Visser, 1997) was included to simulate diffusion (Hunter et al., 1993). This method uses a constant diffusion coefficient in the horizontal direction and a variable diffusion coefficient in the vertical direction. The latter is based on the vertical diffusivity obtained from the turbulence closure model in the hydrodynamics model GETM (see also Sect. 2.2.2). The combined hydrodynamics model (GETM) and particle tracking model (GITM) were applied recently to simulate the transport of plaice larvae in the North Sea (Tiessen et al., 2014).

The biological development and behaviour module of GITM allows particles to progress through a user-defined number of egg and larval development stages. However, these mechanisms were not used here. Instead, the model was modified to include a simplified version of the reproduction mechanism suggested by Salihoglu et al. (2011), elements of which originate from the model of Kremer (1976). This reproduction mechanism was implemented to affect the number of individuals represented by a super-individual (particle). The main simplifications were: (i) each super-individual

OSD
11, 1561–1611, 2014

was assumed to represent a number of adults of average mass; (ii) egg and juvenile stages were assumed to be infinitely short to allow for (i); (iii) food stocks were assumed not to be impacted upon by *M. leidyi*. The reproduction mechanism was implemented as follows; all values and constants were taken from Salihoglu et al. (2011) unless specified otherwise.

Eggs were only produced if temperature and salinity were above the thresholds of 12 °C and 10 PSU, respectively (Lehtiniemi et al., 2012). The number of eggs produced per time step n_e depended on food availability:

$$n_e = \frac{f F_a}{w_e} \tag{1}$$

with F_a the food intake of the adult population represented by the super-individual [mg C timestep^{-1}], $w_e = 0.1$ µg C the average mass of an egg, and f the proportion of food turned into eggs. The adult food intake was calculated as:

$$F_a = n_a \frac{f_a}{1000} c_{cd} w_a G_a A_a \frac{dt}{24 \times 3600} \tag{2}$$

with n_a the number of adults represented by the super-individual, f_a the adult food concentration [mg C m^{-3}] (taken here as mesozooplankton from the GETM-ERSEM-BFM model, see Sect. 2.2.2), $w_a = 2.8$ mg C the average mass of an adult, dt the time step [s], $c_{cd} = 73$ mg mg^{-1} C a factor to convert carbon weight to dry weight, $A_a = 0.72$ the adult assimilation efficiency, and G_a the adult clearance rate [L mg^{-1} dry weight day^{-1}]:

$$G_a = a_0 \left[\left(\frac{w_a}{c_{w2c}} \right)^{-b} \right] e^{kT} \tag{3}$$

with $a_0 = 0.09$ L mg^{-1} d^{-1} an empirical constant, $b = 0.5$ a power, $k = 0.05$ °C^{-1} a decay coefficient, $c_{w2c} = 0.574$ mg C mg^{-1} a conversion factor of wet weight to carbon weight, and T temperature [°C].

OSD
11, 1561–1611, 2014

In Eq. (1), the proportion of food turned into eggs f was calculate as:

$$f = 0.01 T_f e^{c_f (w_a / c_{w2c})} \quad (4)$$

with $c_f = 0.115\,\mathrm{mg}^{-1}$ an empirical constant, and T_f a temperature function given by:

$$T_f = a_T e^{b_T T} \quad (5)$$

with $T_{f,\,min} = 0.01$ a minimum introduced here to prevent negative values, and $a_T = 0.03$ and $b_T = 0.14$ empirical constants. Out of the three functions suggested by Salihoglu et al. (2011) we have chosen this one over the linear function preferred by Salihoglu et al. (2011), which has a cut-off at a rather high temperature of approx. 14 °C. For the reference run example of Salihoglu et al. (2011), the order of magnitude of the number of eggs (several hundreds) produced using these equations corresponded with the observations for small individuals presented by Kremer (1976) and Reeve et al. (1989). Note that a direct comparison is impossible because the conditions of the observations, as far as reported, cannot be fully represented with the current model.

Subsequently, the number of eggs calculated in Eq. (1) was subjected to egg and juvenile mortality. The number of surviving eggs n_{es} was calculated using a constant daily mortality rate $m_e = 0.7$ and assuming an egg phase duration of 1 day:

$$n_{es} = (1 - m_e) n_e \quad (6)$$

Juvenile mortality was calculated as a combination of a daily background mortality $m_j = 0.27$ and food availability. Egg and juvenile daily mortalities were calibrated to reproduce the results of the reference run example of Salihoglu et al. (2011). The surviving juveniles n_{js} after application of the background mortality was:

$$n_{js} = \left(1 - m_j\right)^{D_j} n_{es} \quad (7)$$

with D_j a temperature-driven duration of the juvenile stage in days

$$D_j = a_d + b_d T \quad (8)$$

OSD
11, 1561–1611, 2014

with $a_d = 76.0$ and $b_d = -2.4$ empirical constants based on the graphs presented by Salihoglu et al. (2011).

Juvenile starvation was implemented by comparing the daily food intake F_j with the average daily weight gain w_g required to reach the mass at the end of the transition stage $w_{aj} = 1.5\,\text{mg C}$:

$$w_g = \frac{w_{aj} - w_j}{D_j} \tag{9}$$

with $w_j = 0.13\,\text{mg C}$ the average mass of a juvenile. The daily juvenile food intake was calculated as:

$$F_j = \frac{f_j}{1000} c_{cd} w_j G_j A_j \left(1 - L_j\right) \tag{10}$$

with f_j the juvenile food concentration [mg C m^{-3}] (taken here as microzooplankton from the GETM-ERSEM-BFM model, see Sect. 2.2.2), $A_j = 0.75$ the juvenile assimilation rate, $L_j = 0.06$ a metabolic loss fraction, and G_j the juvenile ingestion rate [$\text{L mg}^{-1}\,\text{day}^{-1}$]:

$$G_j = 0.4 \times 12.3 \times \left(\frac{w_j}{c_{w2c}}\right)^{0.574} + 0.1 \tag{11}$$

Then finally, by combining the results of Eq. (7), (9) and (10), the number of new adults recruited into the existing population (n_{ar}) in the time step under consideration (i.e. assuming infinitely short egg and juvenile duration, but including mortality calculated over their normal duration) was calculated as:

$$n_{ar} = \min\left(1, \frac{F_j}{w_g}\right) n_{js} \tag{12}$$

OSD
11, 1561–1611, 2014

Adults were assumed not to survive temperatures less than 2 °C. For temperatures above that, a background mortality of 2 % was imposed following Salihoglu et al. (2011), and also a daily starvation mortality rate of 13 % for food concentrations less than 3 mg C m^{-3} (Oliveira, 2007). The latter results in approximately 10 % of the population surviving after 17 days.

2.2.2 GETM-ERSEM-BFM

The coupled physical-biogeochemical model GETM-ERSEM-BFM was used to produce hydrodynamics and food fields for the particle tracking model. GETM (General Estuarine Transport Model) is a public domain, three-dimensional finite difference hydrodynamical model (Burchard and Bolding, 2002; www.getm.eu). It solves the 3-D partial differential equations for conservation of mass, momentum, salt and heat. The ERSEM-BFM (European Regional Seas Ecosystem Model - Biogeochemical Flux Model) version used here is a development of the model ERSEM III (see Baretta et al., 1995; Ruardij and Van Raaphorst, 1995; Ruardij et al., 1997; Vichi et al., 2003, 2004, 2007; Ruardij et al., 2005; Van der Molen et al., 2013; www.nioz.nl/northsea_model), and describes the dynamics of the biogeochemical fluxes within the pelagic and benthic environment. The ERSEM-BFM model simulates the cycles of carbon, nitrogen, phosphorus, silicate and oxygen and allows for variable internal nutrient ratios inside organisms, based on external availability and physiological status. The model applies a functional group approach and contains four phytoplankton groups, four zooplankton groups and five benthic groups, the latter comprising four macrofauna and one meiofauna groups. Pelagic and benthic aerobic and anaerobic bacteria are also included. The pelagic module includes a number of processes in addition to those included in the oceanic version presented by Vichi et al. (2007) to make it suitable for temperate shelf seas: (i) a parameterisation for diatoms allowing growth in spring, (ii) enhanced transparent exopolymer particles (TEP) excretion by diatoms under nutrient stress, (iii) the associated formation of macro-aggregates consisting of TEP and diatoms, leading to enhanced sinking rates and a sufficient food supply to the benthic system especially

OSD
11, 1561–1611, 2014

in the deeper offshore areas (Engel, 2000), (iv) a *Phaeocystis* functional group for improved simulation of primary production in coastal areas (Peperzak et al., 1998), and (*v*) a suspended particulate matter (SPM) resuspension module that responds to surface waves for improved simulation of the under-water light climate (see Van der Molen et al., 2014 for details).

2.2.3 Application: North Sea

The GETM-ERSEM-BFM model was run from 1991 until 2009, and hot-started from a 50 year hindcast carried out with an earlier version (Van Leeuwen et al., 2013). Hourly hydrodynamics and food fields were stored from June 2008 to February 2009. The particle tracking model was run from the 1 June 2008 to the 31 January 2009, releasing 3 particles per day from the 1 June until the 30 October in each of 6 grid cells just seaward of the Dutch estuaries, corresponding with expected bloom times (eg., Collingridge et al., 2014). The particles were assumed to be passive tracers. Upon release, each particle was assumed to represent 1000 *M. leidyi* individuals. Daily particle positions, particle characteristics and environmental conditions were stored. The results were processed into density contour maps, and into time series of properties aggregated over all the particles. In the following, this run is called the standard run. To illustrate the effect of temperature on reproduction, and to compare with the response in warmer waters, an additional scenario run was carried out in which the particles experienced 10 % higher temperatures. The sensitivity to juvenile mortality was assessed by a model run with two thirds of juvenile mortality at normal temperatures, and a run with four thirds of juvenile mortality at the 10 % higher temperatures.

To study interconnectivity between ports and estuaries along the French Channel coast and areas in the southern North Sea, a model run was carried out releasing 20 particles per day at one grid cell in the mouth of the river Seine, and one grid cell in the mouth of the river Somme during the same period as in the previous simulations.

OSD
11, 1561–1611, 2014

2.3 Dynamic Energy Budget (DEB) model

2.3.1 DEB model

Dynamic Energy Budget (DEB) theory (Kooijman, 2010) describes the uptake and use of food for all organisms under conditions in which food densities and temperatures vary and applies to all animals. Augustine et al. (2014) carried out a literature review on eco-physiological data for *M. leidyi* and estimated DEB model parameters for this species (see Table 1). The formulation of the standard DEB model applied to *M. leidyi* is well documented in Augustine et al. (2014). We refer to that study for details.

In short in the DEB theory, the state of the individual is quantified by energy fixed in reserve (E, J), volume of the structural component (V, cm^3) and its maturity level (E_H, J), see Fig. 3. The model closes the full life-cycle from egg until adult. Stage transitions are assumed to occur at fixed maturity levels, see Fig. 13a for the definition of the life stages.

Mnemiopsis leidyi is characterized, along with a variety of other species, by a so-called metabolic acceleration during ontogeny, which means that an individual initially has a slow development relative to that of juveniles and adults (Kooijman, 2012, 2014). *Mnemiopsis leidyi* was found to begin to accelerate its metabolism sometime after hatching at maturity level E_H^s. The end of the acceleration was found to coincide with the end of the transitional stage defined in the model as: $E_H = E_H^j$ (Augustine et al., 2014). Metabolic acceleration is defined as an increase in energy conductance and surface-area specific assimilation during that phase; this acceleration is implemented in the model by applying a shape coefficient $(V/V_s)^{1/3}$ where V_s is the structure at the onset of acceleration to both of the parameters designated with an asterix in Table 1.

Food uptake is taken proportional to organism surface area and is converted into reserves with a constant efficiency. A fixed fraction $\kappa \dot{p}_c$ of reserve is mobilised towards growth and somatic maintenance while the remaining fraction $(1-\kappa)\dot{p}_c$ is mobilised towards maturity maintenance plus maturation (in embryos and juveniles) or reproduction

OSD
11, 1561–1611, 2014

(in adults). Somatic maintenance has priority over growth, and hence, growth ceases when $\kappa \dot{p}_c$ no longer suffices to cover somatic maintenance.

2.3.2 Setup and application

The DEB model and parameters presented in Augustine et al. (2014; see Table 1) were used to simulate effects of food and temperature on key life history traits of *M. leidyi*. Food and temperature are treated as forcing variables; reproduction, mass and timing of stage transitions are model output.

We ran two simulation experiments: in the first experiment we computed juvenile stage duration and reproduction rates at different temperatures and for three different scaled functional responses f.

The scaled functional response f relates ingestion to food density in the environment:

$$f = \frac{X}{K + X} \tag{13}$$

$0 < f < 1$ where 0 reflects starvation and 1 optimal food conditions (feeding ad libitum). X is the density of food in the environment ($\mathrm{g\,C\,L^{-1}}$) and K ($\mathrm{g\,C\,L^{-1}}$) is the half saturation coefficient where $K = \frac{\{\dot{F}_\mathrm{m}\}}{\{\dot{J}_\mathrm{XAm}\}}$. $\{\dot{F}_\mathrm{m}\}$ ($\mathrm{l\,d^{-1}\,cm^{-2}}$) is the surface area specific food searching rate. $\{\dot{J}_\mathrm{XAm}\}$ ($\mathrm{mol\,d^{-1}\,cm^{-2}}$) is the maximum surface-area specific ingestion rate. Assuming a digestion efficiency of $\kappa_X = 0.8$, and that food has a chemical potential of $\mu_X = 525\,\mathrm{kJ\,mol^{-1}}$, we can relate $\{\dot{J}_\mathrm{XAm}\}$ to the maximum surface-areas specific assimilation rate $\{\dot{p}_\mathrm{Am}\}$ (a model parameter, see Table 1) by the following relationship: $\{\dot{J}_\mathrm{XAm}\} = \{\dot{p}_\mathrm{Am}\}/\kappa_X/\mu_X$. Thus, K is a very context-specific parameter because it both reflects the capacity of the organism to search for prey, the food quality of the prey and the intrinsic maximum assimilation capacity of the individual. For the purpose of this study we assumed that $\{\dot{F}_\mathrm{m}\} = 4\,\mathrm{L\,d^{-1}\,cm^{-2}}$.

OSD
11, 1561–1611, 2014

All rates and ages were corrected for the effect of temperature using an Arrhenius type relation that describes the rates $\dot{k}(T)$ at ambient temperature, as follows:

$$\dot{k}(T) = \dot{k}(T_1) \times e^{\left[\frac{T_A}{T_1} - \frac{T_A}{T}\right]} \quad (14)$$

where T is the ambient temperature (K), T_A the Arrhenius temperature (K) and $T_1 = 293$ is the reference temperature (K). This relationship assumes that the temperature experienced by the organism is within its tolerance range. Below or above that tolerance range physiological performance starts to be negatively impacted (Kooijman, 2010), but we do not account for this here.

The weight of the organism is computed as the sum of the weights of E and V. We convert volumes and energy to carbon mass using a carbon density of $0.0015\,\mathrm{g\,C\,cm^{-3}}V$, elemental frequencies C : H : O : N taken to be 1 : 1.8 : 0.5 : 0.15 and assuming a chemical potential of E, $\mu_E = 5.50\,\mathrm{kJ\,mol^{-1}}$ (Lika et al., 2011). Age and size at onset of acceleration, end of acceleration, first reproduction are evaluated by integrating over maturity.

3 Results

3.1 Estuaries

The results of the Eastern Scheldt model runs are presented in Table 2 and Fig. 4. The retention within the estuary ranged from 56 % to 66 % (60 % on average), while on average only 10 % of the particles remained in the estuary mouth. The connectivity with the Western Scheldt was low, 2 % on average. No clear seasonal pattern was found.

The final concentration pattern ($\mathrm{m^{-3}}$) for the Eastern Scheldt July simulation is given in Fig. 5. The concentration was calculated by counting the particles within a hydrodynamic grid cell, dividing by the volume, and scaling relative to an assumed initial concentration of $1.0\,\mathrm{m^{-3}}$. Deep in the estuary the concentrations were still close to $1.0\,\mathrm{m^{-3}}$ and no exchange had happened.

OSD
11, 1561–1611, 2014

The results of the Western Scheldt model runs are presented in Table 3 and Fig. 6. The retention within the estuary ranges from 51 % to 69 % per month (65 % on average), while on average 20 % of the particles remained in the estuary mouth. The connectivity with the Eastern Scheldt was low, 2 % per month on average. In general, the retention was larger in summer and autumn than in winter, due to lower river discharges. The final concentration pattern for the July run is given in Fig. 7. Concentrations in the inner part of the estuary were reduced by fresh water inflow from the river Scheldt. The retention was negatively correlated with the river discharge ($r \leq -0.76$, $p < 0.001$).

The sensitivity test for the release time showed an increased retention of 5 % for the Eastern Scheldt July run and a 3 % increase of retention for the Western Scheldt July run. This difference could be explained by the fact that simulations starting at low water begin with inflow, whereas simulations starting at high water begin with outflow.

The results of the realistic run for the Western Scheldt are presented in Fig. 8 as contour plots of *M. leidyi* densities (ind. m^{-3}) as calculated by the model together with the measurements as coloured circles using the same scale. Figure 8a gives the initial condition, which conforms to the observations.

Figure 8b gives the density on the 1 December 2011. There is a good match in the middle of the estuary. At the innermost station there is some overestimation of the concentration. The relative high measurement outside the estuary is not met by the model.

The initial condition and the result on the 20 October 2011 for the Eastern Scheldt run is presented in Fig. 8c and d. The model represented the conditions in the inner estuary reasonably well with some underestimation in the northern branch and some overestimation in the south eastern branch. There is an overestimation of the concentration in the outer part of the estuary.

OSD
11, 1561–1611, 2014

3.2 North Sea

The particles dispersed as a plume along the continental coast to the north, and to a limited extent to the south (Fig. 9). The plume detached from the coast in the vicinity of the Dutch–German border, and continued to the north at some distance from the Danish coast. The particles that travelled furthest reached approximately the middle of the Danish west coast. The concentration of particles decreased steadily along the plume, in response to both the temporal distribution of release and dispersion. The associated density of *M. leidyi* individuals showed a similar pattern, but with a strong reduction in densities in winter in response to adult mortality (Fig. 10).

The model run releasing particles in the rivers Seine and Somme (Fig. 11) resulted in moderate transport to the West up to Cap de la Hague, and substantial transport along the continental coast to the North through the Strait of Dover, along the Dutch coast and into the German Bight. Enhanced concentrations were simulated off the Belgian coast, and *M. leidyi* individuals reached the German Bight, similar to the pattern obtained from releasing particles off the Dutch estuaries, but slightly further offshore. Low numbers crossed the North Sea to the UK and were found in the Thames estuary and off the coast of East Anglia. None of the particles crossed the English Channel south of the Strait of Dover.

For the standard run, the total number of *M. leidyi* individuals increased steadily as particles were released, levelling out in response to the background adult mortality, and declined when starvation set in in December (Fig. 12a, dark blue line). Food abundance for juveniles and adults was high until the beginning of October, and declined to reach low winter values by December (Fig. 12b and c). Average temperature experienced by the particles peaked at 20 °C, declining to winter values of 4 °C (Fig. 12h). Average salinity experienced by the particles increased until the beginning of October, consistent with reduced precipitation in summer and their transport away from the fresh-water source of the river Rhine, and decreased subsequently as river runoff increased in the autumn (Fig. 12i). Over a million eggs were produced per hour by the population in

OSD
11, 1561–1611, 2014

July, August and September (Fig. 12d, dark blue line). However, due to primarily juvenile mortality hardly any new adults were added to the population (Fig. 12e–g). An important factor for juvenile mortality as implemented here is the prolonging of juvenile duration for lower temperatures, leading to strongly reduced overall survival. The scenario run with two thirds of juvenile mortality showed some bloom potential, with new individuals contributing to population growth (Fig. 12, red lines).

The model run in which the particles were made to experience 10 % increased temperatures produced significantly different results. The maximum average temperature experienced by the particles was now approximately 22 °C, with winter temperatures nearly the same as in the reference scenario (Fig. 12h, green line). Over 10 million eggs were produced per hour between the beginning of August and the end of September (Fig. 12d, green line). This caused a bloom that increased the adult population at a rate far greater than the number of the additional particles that were released (Fig. 12a). Increasing the juvenile mortality by one third for this experiment, however, prevented the bloom, and the associated model run thus yielded results very much like those of the standard run (Fig. 12, light blue lines).

For the model run releasing particles in the Seine and the Somme (Fig. 12, magenta lines), the mean concentration of food encountered was slightly lower. Average salinity was higher, indicating a more seaward trajectory of the particles. Egg production and survival was comparable with the standard run, considering that approximately twice as many particles were released. As for the standard run, hardly any adults were added to the population through reproduction.

3.3 DEB model

The DEB model simulations showed that the timing of stage transitions is extremely sensitive to the food level experienced by an individual. Indeed, f can be interpreted as the actual ingestion relative to the maximum possible one for an individual of that size.

OSD
11, 1561–1611, 2014

The model suggested that an individual would mature even when experiencing food levels only 30 % of the maximum – however the time it would theoretically take increases from less than a month to almost three months (Fig. 13a and b).

The duration of metabolic acceleration went from ca 2 weeks to a little over 1.5 months at 22 °C depending on the food history. The predicted mass at the end of the acceleration phase only varied from 0.11 to 0.16 mg C. The adult parameter values depended on the acceleration factor given by the ratios of structure at E_H^j and E_H^s, thus food history has consequent impact on the duration of the acceleration phase, but not so much on the extent of the acceleration which stays around 8.6.

The mass at the different stage transitions was less sensitive to the prior feeding history than timing of the life history events; nonetheless carbon mass at puberty is predicted to go from 1.8 mg C at at libitum feeding to 0.8 mg C at $f = 0.3$ (Fig. 13a).

The DEB model simulations illustrated that growth after puberty was extremely sensitive to food level – the predicted maximum carbon mass went from ca. 80 mg C ($f = 1$) to 2 mg C at $f = 0.3$. Finally, the simulations showed that reproductive output was extremely sensitive to size as well as food history. A 1.8 mg C individual might produce around 1500 eggs d^{-1} at 22 °C while the 0.8 mg C individual would only produce ca. 344 eggs d^{-1} (Fig. 13c).

At low food levels in combination with low temperatures, the organism can stay in the juvenile stage for a very long time: at 12 °C and $f = 0.3$ it could take up to 300 d to reach puberty. Yet the model predicted that at abundant food and temperatures as high as 26 °C reproduction would take as little as 14 d to start in accordance to observations by Baker and Reeve (1974).

The model results indicated that juveniles can maintain themselves at very low environmental food levels and can wait out the bleak season especially if temperatures are low until conditions are favorable for rapid growth and reproduction.

For the second simulation experiment we extracted the temperature and the juvenile and adult food densities experienced by a particle in the GETM-ERSEM-BFM model. The values of the food densities and the temperature can be found in Fig. 14a. By using

OSD
11, 1561–1611, 2014

the relationship (13) we obtain the scaled functional response experience by juveniles and adults (Fig. 14b). The GETM-ERSEM-BFM model predicted that food densities drop in winter. Thus all of the juveniles that were spawned just before the drop in food availability and temperature could potentially be overwintering as juveniles.

In Fig. 14c the reproduction rates for adults of three size classes (2.8, 5 and 10 mg C respectively) were computed. We computed the minimum f needed for each size class to pay its maintenance and found: 0.3, 0.4 and 0.5 for the smallest to the largest individual. Assuming that the organism stops reproducing when f decreases below the minimum f to pay it maintenance we obtain the pattern that larger individuals are more sensitive to drops in food availability but that they also reproduce more when food is abundant enough. In summary, the model predicts rapid response to changes in reproduction as function of food level.

4 Discussion and conclusions

4.1 Interconnectivity

4.1.1 Exchange between estuaries and North Sea

Growth and mortality are not included in the Delft3D model and might explain some of the mismatch between modelled output and field measurements. E.g., better growth conditions in the inner estuary may have caused an underestimation of the modelled numbers in the northern branch of Eastern Scheldt. On the other hand, the overestimation in the modelled numbers in the outer estuary could be explained by the model not considering mortality.

The initial model conditions were based on a small set of measurements, which do not account for potential local patchiness in density. Also, for the Eastern Scheldt, the hydrodynamics used were from a different year. The schematic runs however show

OSD
11, 1561–1611, 2014

little variability between months within the same year, indicating that there might be little variability between the same period in different years.

The results of the Delft3D model indicated that about 10–15 % of the particle released in the Scheldt estuaries were exported to North Sea on monthly basis. This is enough for a substantial supply of *M. leidyi* to coastal waters of the North Sea on one hand, and on the other hand allows for sufficient retention in the estuaries to facilitate blooms and an overwintering population. The model suggested an increasing level of retention towards the landward end of the estuaries, which contributes to this mechanism. A similar process has been described in other estuaries, such as Narragansett bay, where shallow, shoreward embayments serve as winter refugia for *M. leidyi* (Costello et al., 2006a,b).

M. leidyi densities in the Eastern Scheldt were a factor 10–100 higher than in the Western Scheldt, and hence the Eastern Scheldt may be a more important source of *M. leidyi* for the coastal waters of the North Sea than the Western Scheldt. A likely explanation for this is that the low salinity levels in part of the Western Scheldt (Meire et al., 2005) are known to limit reproduction (Jaspers et al., 2011) and increase larval mortality (Lehtiniemi et al., 2012).

4.1.2 Exchange between coastal areas

The GITM particle tracking IBM suggested a general south to north transport along the continental coast, in agreement with the residual flow pattern (e.g., numerical model: Prandle, 1978; radioactive tracers: kautsky, 1973; various data: North Sea Task Force, 1993). As a result, any estuary or harbour containing an established *M. leidyi* population can, within one year, act as a source area for estuaries and harbours along the coast to the north at distances of tens to many hundreds of kilometres. For colonisation at larger distances, *M. leidyi* will need to establish a year-round population in one of the receiving coastal embayments, which can then in turn act as a source population in the following year. As a result, *M. leidyi* will be able to survive in the connected network of estuaries tens to hundreds of kilometres apart, as long as there is intermittent

OSD
11, 1561–1611, 2014

winter survival in some of them each year. Although there is occasional transport of *M. leidyi* individuals over limited distances to the southwest, a solidly established, continuous population in the southernmost estuary or harbour in the chain is also likely to be required.

To our knowledge, *M. leidyi* has so far not been found in the UK. The model results suggested only minor potential for *M. leidyi* to colonise UK waters through natural transport processes from continental populations. The most likely stretch of UK coast vulnerable to colonisation appeared to be the East Anglian coastline. As the general residual coastal flow converges from north and south in this area, and then moves across the North Sea towards Scandinavia, *M. leidyi* is not expected to be able to colonise further along the UK coast through natural transport processes should it be able to establish itself in East Anglia.

4.2 Comparison DEB model and IBM *M. leidyi* implementation

There is a need to work with simple characterizations of metabolism when performing ecosystem level modelling. The way the biology of *M. Leidyi* was implemented into particle tracking models in this study is a promising way to proceed. But it also becomes difficult to assess what would happen to the output if more complex, albeit more realistic aspects of the individual physiology (e.g. growth) were incorporated. Would such implementations pay off in terms of adding new insight?

The simulation studies with the DEB model show how sensitive the juvenile stage duration and reproduction rates are likely to be to differences in food availability and temperature. In light of the predicted plasticity in growth and juvenile stage duration, future studies should consider incorporating these processes.

It is not clear to which extent the timing of the juvenile stage is realistic because there is no clear empirical evidence about how stage duration depends on different food levels, however, the values obtained here for juvenile stage duration are within the range presented in other studies: Baker and Reeve (1974) predict timing of first reproduction to be 13–14 d at 26 °C, Jaspers (2012; Chap. 6, Fig. 1a) show that reproduction

OSD
11, 1561–1611, 2014

is starting around 22–32 days at 19.5 °C (the DEB model with parameters in Table 1 predicts 30 d).

The DEB model was shown to constitute a quantitative characterization of the baseline metabolism of the species (Augustine et al., 2014). Model predictions for reproduction rates and mass as function of length are in accordance with reproduction rates against length and wet mass reported in Baker and Reeve (1974); Jaspers (2012; Chap. 6, Fig. 2, circles) and Kremer (1976; Fig. 2) respectively. We refer the reader to Augustine et al., 2014, where model predictions are compared with these data sets and the model results are discussed in more detail.

Separate juvenile and adult food densities were extracted from the GETM-ERSEM-BFM model in line with the model proposed by Salihoglu (2011), based on observations and physiology. The juvenile period, incl. the food availability, is fully accounted for in transitioning eggs into adults in the particle tracking model, i.e. if the juvenile period is long, or food levels are low, fewer make it into adulthood because of mortality. However, in terms of the time stepping in the model, this whole transition happens (artificially) in one time step (1 h).

It is difficult to conclude how exactly the energy assimilated by the growing individual relates to the carbon mass density of different size classes of zooplankton as predicted by the ERSEM model. Running the DEB model allowed us to uncouple the problem of effects of varying resources on the metabolism from the problem of how food availability relates to assimilation rates. It turns out that with this set of parameter values for *Mnemiopsis* juveniles seem to experience high food levels relative to adults (Fig. 14b). We see from Fig. 14c that the size structure of the population could strongly impact the dynamics of reproduction.

The value one choses for the food searching rate will also determine how much energy is assimilated by the organism. We chose the value of $4\,\mathrm{L\,d^{-1}\,cm^{-2}}$, for the sake of the simulation studies herein, but it is unclear whether or not a unique value can be used.

OSD
11, 1561–1611, 2014

Uncertainties about reproduction rates further hamper finding good estimates for juvenile mortality. Still too little is known about what natural processes affect juvenile mortality in the field. And our study only exacerbates to what extent we need to know more about this. Are the processes similar to those involved in the regulation of fish recruitment?

Comparison between the two models, as far as possible with the current results, illustrates that although there are similarities, there are also substantial differences. These differences are partly due to the values chosen for key parameters, which, at the current state of knowledge, include substantial uncertainty. They are also partly caused by the more sophisticated processes included in the DEB model. There is clearly room for improvement, for instance in the shape of a particle tracking model with particles that represent "real" individuals through use of a DEB model for each particle, and that can spawn independent new particles as offspring. Such a model is likely to produce results that differ substantially from the current particle tracking model, and that may be more realistic. Reducing uncertainty in parameter values through observational and laboratory studies is vital, however, to ensure the required level of confidence in such a model.

4.3 Survival and reproduction in the North Sea

The simulations indicated that food levels in coastal waters in the North Sea were sufficient to sustain a *M. leidyi* population in summer and a reduced population until mid-winter. Current offshore water temperatures were too low in summer and autumn for *M. leidyi* to reproduce in large numbers. The presence of *M. leidyi* found near the German Bight corresponded with observations of *M. leidyi* in mid-winter in these waters on the IBTS cruises and results from a habitat model on winter survival (David et al., 2014; Antajan et al., 2014). These results are, however, subject to considerable uncertainty due to the unknown effects of (juvenile) mortality that dominate the reproduction process, and to potential adaptation to lower temperatures. In particular, production of eggs at temperatures too low for juvenile survival does not seem to make evolutionary

OSD
11, 1561–1611, 2014

sense, suggesting that juvenile mortality may be temperature-related, rather than constant as assumed in the particle tracking IBM. Further work is required to elucidate these issues.

The scenario simulation with increased summer temperatures suggested that water temperature is an important limiting condition for blooms in the North Sea. The model results suggest that blooms may occur in some years as a result of interannual variability in temperature, and that such incidences may increase in frequency in the future as a result of global warming. This result is consistent with the parameterisations in the model, and with observed reproduction behaviour in warmer seas (Shiganova et al., 2001). Moreover, blooms tend to be found in estuaries, which experience higher water temperatures the surrounding seas (Costello et al., 2006a, b). The simulated blooms for the increased temperature scenario should be considered an upper estimate, as food concentrations are not impacted on by grazing of *M. leidyi* in the present model implementation. Other limiting conditions such as predation may exist as well, but these were not included in the model.

Acknowledgements. This work was performed within the MEMO project "*Mnemiopsis* ecology and modeling: observation of an invasive comb jelly in the North Sea" (06-008-BE-MEMO), which is a crossborder cooperation, funded by the European Interreg IVA 2 Seas program.

S. Augustine was supported by the Danish Research Council and the HCØ scholarship. The Centre for Ocean Life is a VKR center of excellence supported by the Villum Foundation.

References

Antajan, E., Bastian, T., Raud, T., Brylinski, J.-M., Hoffman, S., Breton, G., Cornille, V., Delegrange, A., and Vincent, D.: The invasive ctenophore *Mnemiopsis leidyi* A. Agassiz, 1865 along the English Channel and the North Sea French coasts: another introduction pathway in northern European waters?, Aquatic Invasions, 9, 167–173, doi:10.3391/ai.2014.9.2.05, 2014.

OSD
11, 1561–1611, 2014

Augustine, S., Jaspers, C., Kooijman, S. A. L. M., Carlotti, F., Poggiale, J.-C., Freitas, V., van der Veer, H., and van Walraven, L.: Mechanisms underlying the metabolic exibility of an invasive comb jelly, J. Sea Res., submitted, 2014.

Baker, L. D. and Reeve, M. R.: Laboratory Culture of the Lobate Ctenophore *Mnemiopsis mccradyi* with Notes on Feeding and Fecundity, Mar. Biol., 26, 57–62, 1974.

Baretta, J. W., Ebenhöh, W., and Ruardij, P.: The European Regional Seas Ecosystem Model, a complex marine ecosystem model, J. Sea Res., 33, 233–246, 1995.

Boersma, M., Malzahn, A., Greve, W., and Javidpour, J.: The first occurrence of the ctenophore *Mnemiopsis leidyi* in the North Sea, Helgoland Mar. Res., 61, 153–155, doi:10.1007/s10152-006-0055-2, 2007.

Bolle, L. J., Dickey-Collas, M., Van Beek, J. K. L., Erftemeijer, P. L. A., Witte, J. I. J., Van der Veer, H. W., and Rijnsdorp, A. D.: Variability in transport of fish eggs and larvae, III. Effects of hydrodynamics and larval behaviour on recruitment in plaice, Mar. Ecol. Progr. Ser., 390, 195–211, 2009.

Brown, J., Hill, A. E., Fernand, L., and Horsburgh, K. J.: Observations of a seasonal jet-like circulation in the central North Sea cold pool margin, Est. Coast. Shelf Sci., 48, 343–355, 1999.

Burchard, H. and Bolding, K.: GETM – a general estuarine transport model, Scientific documentation, Tech. Rep. EUR 20253 EN, European Commission, 2002.

Collingridge, K., Van der Molen, J., and Pitois, S.: Modelling risk areas in the North Sea for blooms of the invasive comb jelly *Mnemiopsis leidyi*, Aquatic Invasions, 9, 21–36, 2014.

Costello, J. H., Sullivan, B. K., and Gifford, D. J.: A physical-biological interaction underlying variable phenological responses to climate change by coastal zooplankton, J. Plankt. Res., 28, 1099–1105, 2006a.

Costello, J. H., Sullivan, B. K., Gifford, D. J., van Keuren, D., and Sullivan, L. J.: Seasonal refugia, shoreward thermal amplification, and metapopulation dynamics of the ctenophore *Mnemiopsis leidyi* in Narragansett Bay, Rhode Island, Limnol. Oceanogr., 51, 1819–1831, 2006b.

David, C., Vaz, S., Loots, C., Antajan, E., van der Molen, J., and Travers-Trolet, M.: Understanding winter distribution and transport pathways of the invasive ctenophore *Mnemiopsis leidyi* in the North Sea: coupling habitat and dispersal modelling approaches, Biol. Invasions, submitted, 2014.

OSD
11, 1561–1611, 2014

Davies, A. M., Kwong, S. C. M., and Flather, R. A.: Formulation of a variable-function three-dimensional model, with application to the M_2 and M_4 tide on the North-West European Continental Shelf, Cont. Shelf Res., 17, 165–204, 1997.

Dickey-Collas, M., Bolle, L. J., Van Beek, J. K. L., and Erftemeijer, P. L. A.: Variability in transport of fish eggs and larvae, II. The effects of hydrodynamics on the transport of Downs herring larvae, Mar. Ecol. Progr. Ser., 390, 183–194, 2009.

Dumoulin, E.: De Leidy's ribkwal (*Mnemiopsis leidyi* (A. Agassiz, 1865)) al massaal in het havengebied Zeebrugge-Brugge, of: exoten als de spiegel van al tè menselijk handelen, De Strandvlo, 27, 44–60, 2007.

Dyer, K. R. and Moffat, T. J.: Fluxes of suspended matter in the East Anglian plume, Southern North Sea, Cont. Shelf Res., 18, 1311–1331, 1998.

Ellis, J. R., Milligan, S. P., Readdy, L., Taylor, N., and Brown, M. J.: Spawning and nursery grounds of selected fish species in UK waters, Centre for Environment Fisheries and Aquaculture Science (CEFAS), CEFAS Science Series Technical Report, 147, Lowestoft, 56 pp., 2011.

Engel, A.: The role of transparent exopolymer particles (TEP) in the increase in apparent particle stickiness (α) during the decline of a diatom bloom, J. Plankt. Res., 22, 485–497, 2000.

Faasse, M. A. and Bayha K. M.: The ctenophore *Mnemiopsis leidyi* A. Agassiz 1865 in coastal waters of the Netherlands: an unrecognized invasion?, Aquat. Invasions, 1, 270–277, 2006.

Flather, R. A.: Estimates of extreme conditions of tide and surge using a numerical model of the North-west European Continental Shelf, Est., Coast. Shelf Sci., 24, 69–93, 1987.

Fuentes, V., Angel, D., Bayha, K., Atienza, D., Edelist, D., Bordehore, C., Gili, J. M., and Purcell, J.: Blooms of the invasive ctenophore, *Mnemiopsis leidyi*, span the Mediterranean Sea in 2009, Hydrobiology, 645, 23–37, 2010.

GESAMP (IMO/FAO/UNESCO_IOC/WMO/WHO/IAEA/UN/UNEP Joint Group of Experts on the Scientific Aspects of the Marine Environmental Protection): Opportunistic Settlers and the Problem of the Ctenophore *Mnemiopsis Leidyi* Invasion in the Black Sea, GESAMP reports and studies No 58, International Maritime Organization, London, 1997.

Hill, A. E., Brown, J., Fernand, L., Holt, J., Horsburgh, K. J., Proctor, R., Raine, R., and Turrell, W. R.: Thermohaline circulation of shallow tidal seas, Geophys. Res. Letters, 35, L11605, doi:10.1029/2008GL033459, 2008.

Hunter, J. R., Craig, P. D., and Philips, H. E.: On the use of random walk models with spatially variable diffusivity, J. Computat. Phys., 106, 366–376, 1993.

OSD
11, 1561–1611, 2014

Hydrographical Survey: Tidal heights and streams, Coastal waters of the Netherlands and adjacent areas, Royal Dutch Navy, Hydrographical Survey, HP33, 308 pp., 2000.
Ivanov, V. P., Kamakin, A. M., Ushivtzev, V. B., Shiganova, T., Zhukova, O., Aladin, N., Wilson, S. I., Harbison, G. R., and Dumont, H. J.: Invasion of the Caspian Sea by the comb jellyfish *Mnemiopsis leidyi* (Ctenophora), Biol. Invasions, 2, 255–258, 2000.
Jaspers, C.: Ecology of gelatinous plankton with emphasis on feeding interactions, distribution pattern and reproduction biology of *Mnemiopsis leidyi* in the Baltic Sea, Ph.D. thesis, National Institute of Aquatic Resources, Technical University of Denmark, 2012.
Jaspers, C., Møller, L. F., and Kiørboe, T: Salinity gradient of the Baltic Sea limits the reproduction and population expansion of the newly invaded comb Jelly *Mnemiopsis leidyi*, PLoS ONE, 6, e24065, doi:10.1371/journal.pone.0024065, 2011.
Kautsky, H.: The distribution of the radio nuclide Caesium 137 as an indicator for North Sea watermass transport, Deutsche Hydrogr. Zeitschr., 26, 241–246, 1973.
Kideys A. E.: Fall and rise of the Black Sea ecosystem, Science, 297, 1482–1484, 2002.
Kooijman, S. A. L. M.: Dynamic Energy Budget Theory for metabolic organization, Cambridge Univ. Press, 2010.
Kooijman, S. A. L. M.: The evolution of metabolic acceleration in animals, J. Sea Res., in press, 2014.
Kooijman, S. A. L. M., Pecquerie, L., Augustine, S., and Jusup, M.: Scenarios for acceleration in fish development and the role of metamorphosis, J. Sea Res., 66, 419–423, 2011.
Kremer, P.: Population dynamics and ecological energetics of a pulsed zooplankton predator, the ctenophore *Mnemiopsis leidyi*, in: Estuarine Processes Vol. I: Uses, Stresses and Adaptation to the Estuary, edited by: Wiley, M., Academic Press, London, 197–215, 1976.
Lehtiniemi, M., Lehmann, A., Javidpour, J., and Myrberg, K.: Spreading and physico-biological reproduction limitations of the invasive American comb jelly *Mnemiopsis leidyi* in the Baltic Sea, Biol. Invasions, 14, 341–354, doi:10.1007/s10530-011-0066-z, 2012.
Lesser, G. R., Roelvink, J. A., Van Kester, J. A. T. M., and Stelling, G. S.: Development and validation of a three-dimensional morphological model, Coast. Eng., 51, 883–915, 2004.
Lika, K., Kearney, M. R., Freitas, V., van der Veer, H. W., van der Meer, J., Wijsman, J. W. M., Pecquerie, L., and Kooijman, S. A. L. M.: The "covariation method" for estimating the parameters of the standard Dynamic Energy Budget model I: philosophy and approach, J. Sea Res., 66, 270–277, 2011.

OSD
11, 1561–1611, 2014

Los, F. J., Villars, M. T., and Van der Tol, M. W. M.: A 3-dimensional primary production model (BLOOM/GEM) and its applications to the (southern) North Sea (coupled physical-chemical-ecological model), J. Marine Syst., 74, 259–294, 2008.
Meire, P., Ysebaert, T., Van Damme, S., Van Den Bergh, E., Maris, T., and Struyf, E.: The Scheldt estuary: a description of a changing ecosystem, Hydrobiol., 540, 1–11, 2005.
North Sea Task Force: North Sea Quality Status Report 1993, Oslo and Paris Commissions, London, Olsen and Olsen, Frendensborg, Denmark, 132 pp., 1993.
Oliveira, O. M. P.: The presence of the ctenophore *Mnemiopsis leidyi* in the Oslofjorden and considerations on the initial invasion pathways to the North and Baltic Seas, Aquat. Invasions, 2, 185–189, 2007.
Otto, L., Zimmerman, J. T. F., Furnes, G. K., Mork, M., Saetre, R., and Becker, G.: Review of the physical oceanography of the North Sea, Neth, J. Sea Res., 26, 161–238, 1990.
Peperzak, L., Colijn, F., Gieskes, W. W. C., and Peeters, J. C. H.: Development of the diatom-Phaeocystis spring bloom in the Dutch coastal zone of the North Sea: the silicon depletion vs. the daily irradiance threshold hypothesis, J. Plankt. Res., 20, 517–537, 1998.
Postma, L., Van Beek, J. K. L., van den Boogaard, H. F. P., and Stelling, G. S.: Consistent and efficient particle tracking on curvilinear grids for environmental problems, Int. J. Num. Meth. Fluids, 71, 1226–1237, 2013.
Prandle, D.: Residual flows and elevations in the southern North Sea, P. Roy. Soc. Lond Ser. A, 359, 189–228, 1978.
Purcell, J. E., Shiganova, T. A., Decker, M. B., and Houde, E. D.: The ctenophore *Mnemiopsis* in native and exotic habitats: US estuaries vs. the Black Sea basin, Hydrobiologia, 451, 145–176, 2001.
Reeve, M. R., Syms, M. A., and Kremer, P.: Growth dynamics of a ctenophore (*Mnemiopsis*) in relation to variable food supply. I. Carbon biomass, feeding, egg production, growth and assimilation efficiency, J. Plankt. Res., 11, 535–552, 1989.
Ruardij, P. and Van Raaphorst, W.: Benthic nutrient regeneration in the ERSEM-BFM ecosystem model of the North Sea, Neth. J. Sea Res., 33, 453–483, 1995.
Ruardij, P., Van Haren, H., and Ridderinkhof, H.: The impact of thermal stratification on phytoplankton and nutrient dynamics in shelf seas: a model study, J. Sea Res., 38, 311–331, 1997.

OSD
11, 1561–1611, 2014

Ruardij, P., Veldhuis, M. J. W., and Brussaard, C. P. D.: Modeling the bloom dynamics of the polymorphic phytoplankter *Phaeocystis globosa:* impact of grazers and viruses, Harmf. Alg., 4, 941–963, 2005.

Salihoglu, B., Fach, B. A., and Oguz, T.: Control mechanisms on the ctenophore *Mnemiopsis* population dynamics: a modelling study, J. Marine Syst., 87, 55–65, 2011.

Schrum, C.: Thermohaline stratification and instabilities at tidal mixing fronts: results of an eddy resolving model for the German Bight, Cont. Shelf Res., 17, 689–716, 1997.

Shiganova, T. A.: Invasion of the Black Sea by the ctenophore *Mnemiopsis leidyi* and recent changes in pelagic community structure, Fish. Oceanogr., 7, 305–310, 1998.

Shiganova, T. A., Mirzoyan, Z. A., Studenikina, E. A., Volovik, S. P., Siokou-Frangou, I., Zervoudaki, S., Christou, E. D., Skirta, A. Y., and Dumont, H. J.: Population development of the invader ctenophore *Mnemiopsis leidyi*, in the Black Sea and in other seas of the Mediterranean basin, Mar. Biol., 139, 431–445, 2001.

Smaal, A. C. and Nienhuis, P. H.: The eastern Scheldt (the Netherlands), from an estuary to a tidal bay: a review of responses at the ecosystem level, J. Sea Res., 30, 161–173, 1992.

Sullivan, L. J. and Gifford, D. J.: Diet of the larval ctenophore *Mnemiopsis leidyi* A. Agassiz (Ctenophora, Lobata), J. Plankton Res., 26, 417–431, 2004.

Tiessen, M. C. H., Fernard, L., Gerkema, T., van der Molen, J., Ruardij, P., and van der Veer, H. W.: Numerical modelling of physical processes governing larval transport in the southern North Sea, Ocean Sci., 10, 357–376, doi:10.5194/os-10-357-2014, 2014.

Undén, P., Rontu, L., Järvinen, H., Lynch, P., Calvo, J., Cats, G., Cuxart, J., Eerola, K., Fortelius, C., Garcia-Moya, J. A., Jones, C., Lenderlink, G., McDonald, A., McGrath, R., Navascues, B., Woetman Nielsen, N., Ødegaard, V., Rodriguez, E., Rummukainen, M., Rõõm, R., Sattler, K., Hansen Sass, B., Savijärvi, H., Wichers Schreur, B., Sigg, R., The, H., and Tijm, A.: HIRLAM-5 Scientific Documentation, HIRLAM-5 Project, available at: http://hirlam.org/ (last access: 12 June 2014), 2002.

Van der Molen, J., Aldridge, J. N., Coughlan, C., Parker, E. R., Stephens, D., and Ruardij, P.: Modelling marine ecosystem response to climate change and trawling in the North Sea, Biogeochem., 113, 213–236, doi:10.1007/s10533-012-9763-7, 2013.

Van der Molen, J., Smith, H. C. M., Lepper, P., Limpenny, S., and Rees, J.: Predicting the large-scale consequences of offshore wind array development on a North Sea ecosystem, Cont. Shelf Res., doi:10.1016/j.csr.2014.05.018, in press, 2014.

OSD
11, 1561–1611, 2014

Van Ginderdeuren, K., Hostens, K., Hoffman, S., Vansteenbrugge, L., Soenen, K., De Blauwe, H., Robbens, J., and Vincx, M.: Distribution of the invasive ctenophore *Mnemiopsis leidyi* in the Belgian part of the North Sea, Aquatic Invasions, 7, 163–169, 2012.

Van Kessel, T., Winterwerp, H., Van Prooijen, B., Van Ledden, M., and Borst, W.: Modelling the seasonal dynamics of SPM with a simple algorithm for the buffering of fines in a sandy seabed, Cont. Shelf Res., 31, 124–134, 2011.

Van Leeuwen, S. M., Van der Molen, J., Ruardij, P., Fernand, L., and Jickells, T.: Modelling the contribution of deep chlorophyll maxima to annual primary production in the North Sea, Biogeochemistry, 113, 137–152, doi:10.1007/s10533-012-9704-5, 2013.

Vansteenbrugge, L., Van Regenmortel, T., De Troch, M., Vincx, M., and Hostens, K.: Gelatinous zooplankton in the Belgian part of the North Sea and the adjacent Schelde estuary: a real problem?, J. Sea Res., submitted, 2014.

Vichi, M., May, W., and Navarra, A.: Response of a complex ecosystem model of the northern Adriatic Sea to a regional climate change scenario, Clim. Res., 24, 141–158, 2003.

Vichi, M., Ruardij, P., and Baretta, J. W.: Link or sink: a modelling interpretation of the open Baltic biogeochemistry, Biogeosciences, 1, 79–100, doi:10.5194/bg-1-79-2004, 2004.

Vichi, M., Pinardi, N., and Masina, S.: A generalized model of pelagic biogeochemistry for the global ocean ecosystem, Part I: Theory, J. Marine Syst., 64, 89–109, 2007.

Vinogradov, M. E., Shushkina, E. A., Musayeva, E. I., and Sorokin, P. Y.: A new exotic species in the Black Sea: the ctenophore *Mnemiopsis leidyi* (Ctenophora: Lobata), Oceanology, 29, 220–224, 1989.

Visser, A. W.: Using random walk models to simulate the vertical distribution of particles in a turbulent water column, Mar. Ecol.-Prog. Ser., 158, 275–281, 1997.

Visser, M.: On the distribution of suspended matter and the density driven circulation in the Dutch coastal area, in: Dynamics and Exchanges in Estuaries and the Coastal Zone, Coastal Estuarine Studies, edited by: Prandle, D., 40, AGU, Washington DC, 551–576, 1992.

Wolk, F.: Three-dimensional Lagrancian tracer modelling in Wadden Sea areas, Diploma thesis, Carl von Ossietzky University Oldenburg, Hamburg, Germany, 85 pp., 2003.

OSD
11, 1561–1611, 2014

Table 1. DEB model parameters used in the simulations. The parameter values are taken from Augustine et al. in prep. * denotes parameters which increase by a factor 8.6 during metabolic acceleration (i.e. $E_H^s < E_H < E_H^j$). The values are given at reference temperature of 20 °C. We refer the reader to Fig. 1 and to the original study (Augustine et al., 2014) for the physiological interpretation of the parameters.

E_H^b	1.5×10^{-3} J	κ	0.7	$\dot{k}_J$	$0.002\ d^{-1}$
E_H^s	4.4×10^{-3} J	κ_R	0.95	$\dot{v}^*$	$0.21\ cm\ d^{-1}$
E_H^j	3.2 J	$[\dot{p}_M]$	$5.0\ J\ cm^{-3}\ d^{-1}$	$\{\dot{p}_{Am}\}^*$	$3.0\ J\ cm^{-2}\ d^{-1}$
E_H^p	42.0 J	$[E_G]$	$78.0\ J\ cm^{-3}$	T_A	1.05×10^4

OSD
11, 1561–1611, 2014

Table 2. Percentage of particles from the Eastern Scheldt estuary per area after 30 days.

	Eastern Scheldt	Western Scheldt	Eastern Scheldt mouth	Western Scheldt mouth	Zeebrugge area	rest North Sea
Jan	62.72	0.32	14.78	3.20	0.00	18.98
Feb	63.72	2.49	13.40	3.76	0.12	16.52
Mar	55.57	2.43	12.91	13.50	0.29	15.30
Apr	62.66	2.90	9.58	10.67	0.32	13.88
May	61.62	3.41	5.54	11.14	0.38	17.92
Jun	57.59	2.32	11.64	12.63	0.17	15.66
Jul	58.64	2.06	8.33	14.96	0.27	15.73
Aug	59.95	1.57	10.92	12.06	0.01	15.49
Sep	62.40	3.55	7.04	15.01	0.46	11.54
Oct	59.81	2.56	8.84	15.16	0.03	13.60
Nov	61.22	2.50	6.94	18.30	0.24	10.80
Dec	61.68	2.66	5.25	14.00	0.27	16.1

OSD
11, 1561–1611, 2014

Table 3. Percentage of particles from the Western Scheldt estuary per area after 30 days.

	Eastern Scheldt	Western Scheldt	Eastern Scheldt mouth	Western Scheldt mouth	Zeebrugge area	rest North Sea
Jan	1.88	57.96	2.62	15.25	0.03	22.26
Feb	0.45	64.59	7.39	12.80	0.24	14.54
Mar	1.04	50.71	5.23	28.31	0.68	14.03
Apr	0.00	66.73	3.09	18.80	0.24	11.13
May	0.00	69.13	0.00	20.60	0.38	9.90
Jun	0.04	65.69	0.61	22.49	0.18	11.00
Jul	0.06	66.78	0.20	22.80	0.33	9.83
Aug	0.77	65.84	1.41	20.08	0.07	11.82
Sep	0.04	68.75	0.08	20.70	0.49	9.93
Oct	0.28	67.14	1.04	20.19	0.16	11.20
Nov	0.55	66.32	0.22	22.61	0.46	9.84
Dec	0.03	64.76	0.16	20.88	0.50	13.65

OSD
11, 1561–1611, 2014

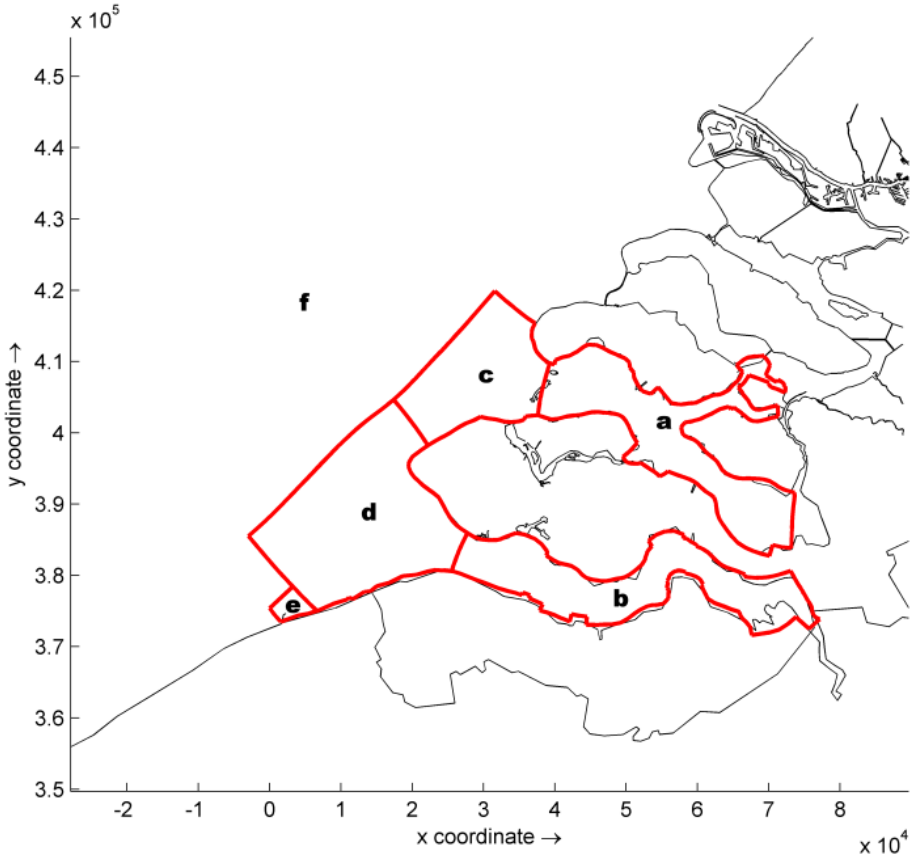

Figure 1. Definition of the areas. **(a)** Eastern Scheldt estuary, **(b)** Western Scheldt estuary, **(c)** Eastern Scheldt mouth, **(d)** Western Scheldt mouth, **(e)** Zeebrugge harbour area and **(f)** other North Sea.

OSD
11, 1561–1611, 2014

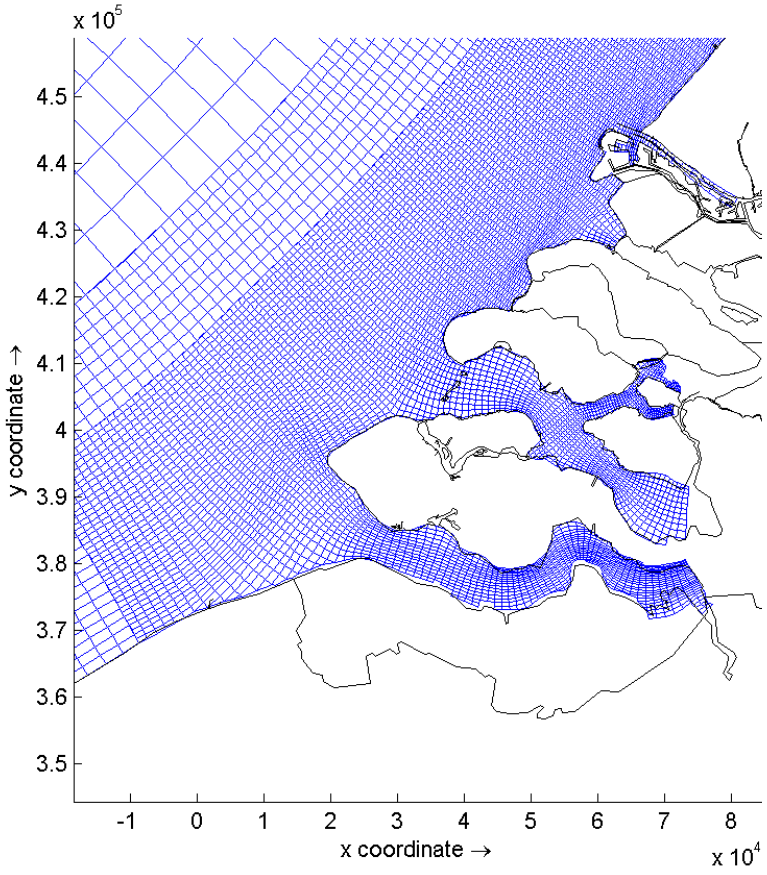

Figure 2. Model grid.

OSD
11, 1561–1611, 2014

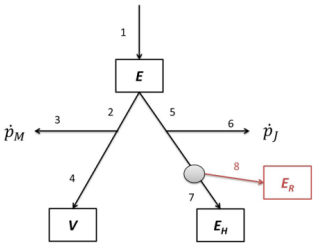

$$\frac{dV}{dt} = \frac{\dot{p}_G}{[E_G]}$$

$$\frac{dE}{dt} = \dot{p}_A - \dot{p}_C$$

$$\frac{dE_H}{dt} = \dot{p}_H$$

$$\frac{dE_R}{dt} = \kappa_R \dot{p}_R$$

1 assimilation: $\dot{p}_A = f\{\dot{p}_{Am}\}V^{2/3}$

2 allocation fraction to soma: $\kappa\, \dot{p}_c$ and $\dot{p}_c = E\,(\dot{v}V^{-1/3} - \frac{\kappa E \dot{v} V^{-1/3} - [\dot{p}_M]V}{\kappa E + [E_G]V})$

3 somatic maintenance costs: $\dot{p}_M = [\dot{p}_M]V$

4 growth (synthesis of structure): $\dot{p}_G = \kappa\, \dot{p}_c - \dot{p}_M$

5 allocation fraction to maturation/reproduction: $(1-\kappa)\, \dot{p}_c$

6 maturity maintenance costs: $\dot{p}_J = \dot{k}_J E_H$

7 maturation: $\dot{p}_H = (1-\kappa)\, \dot{p}_c - \dot{p}_J$ if $E_H < E_H^p$ else $\dot{p}_H = 0$

8 reproduction: $\dot{p}_R = (1-\kappa)\, \dot{p}_c - \dot{p}_J$ if $E_H = E_H^p$ else $\dot{p}_R = 0$

Figure 3. Energy flux scheme of the standard DEB model. Boxes: variables. Arrows: energy fluxes in J d^{-1}. The equations for each flux can be found below. Grey circle: metabolic switch associated with puberty: the individual stops allocating towards maturation and starts allocating towards puberty. E_X: food (J), E_P: faeces (J), E: reserve (J), V: volume of structure (cm^3), E_H: cumulated energy invested in maturation, and E_R: cumulated energy invested in reproduction. The energy fluxes are functions of the model parameters which can be found in Table 1.

OSD
11, 1561–1611, 2014

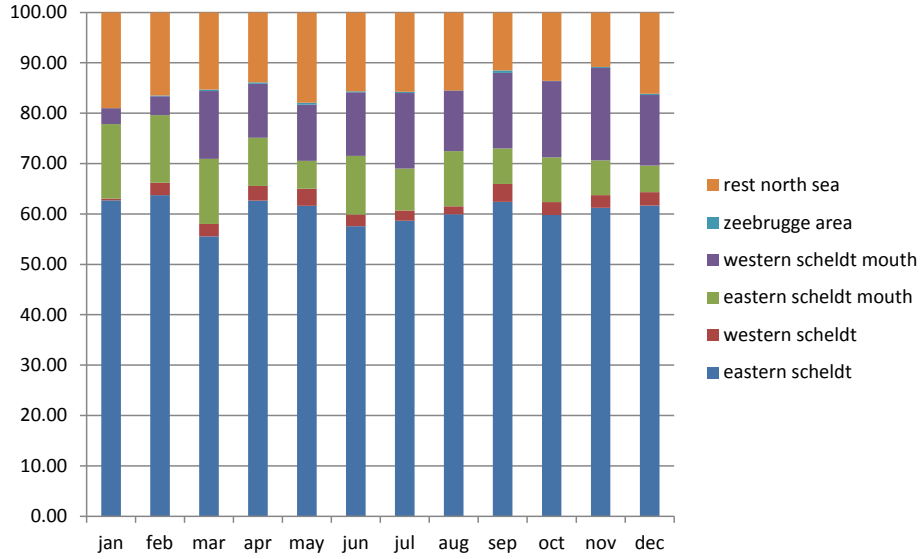

Figure 4. Percentage of particles from the Eastern Scheldt estuary per area after 30 days.

OSD
11, 1561–1611, 2014

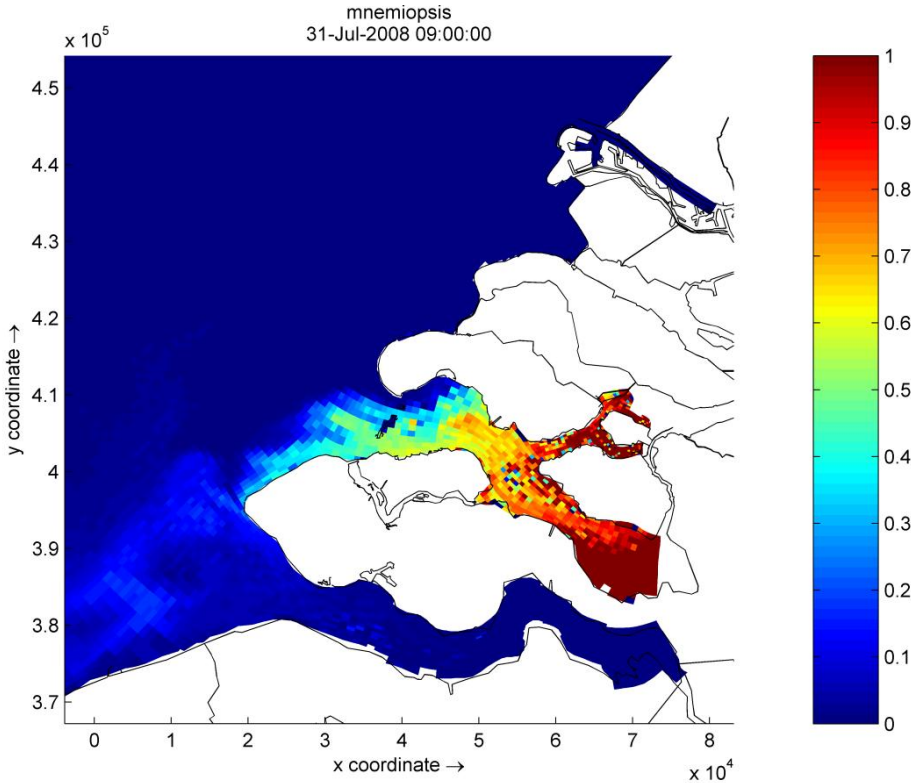

Figure 5. Final concentration ($N\,m^{-3}$) relative to an assumed initial concentration of 1.0 ($N\,m^{-3}$) for the Eastern Scheldt July simulation.

OSD
11, 1561–1611, 2014

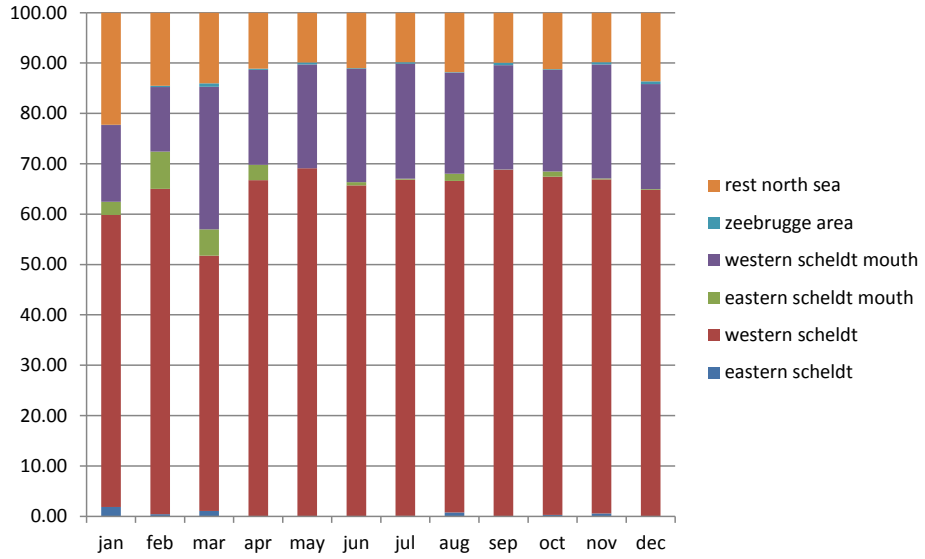

Figure 6. Percentage of particles from the Western Scheldt estuary per area after 30 days.

OSD
11, 1561–1611, 2014

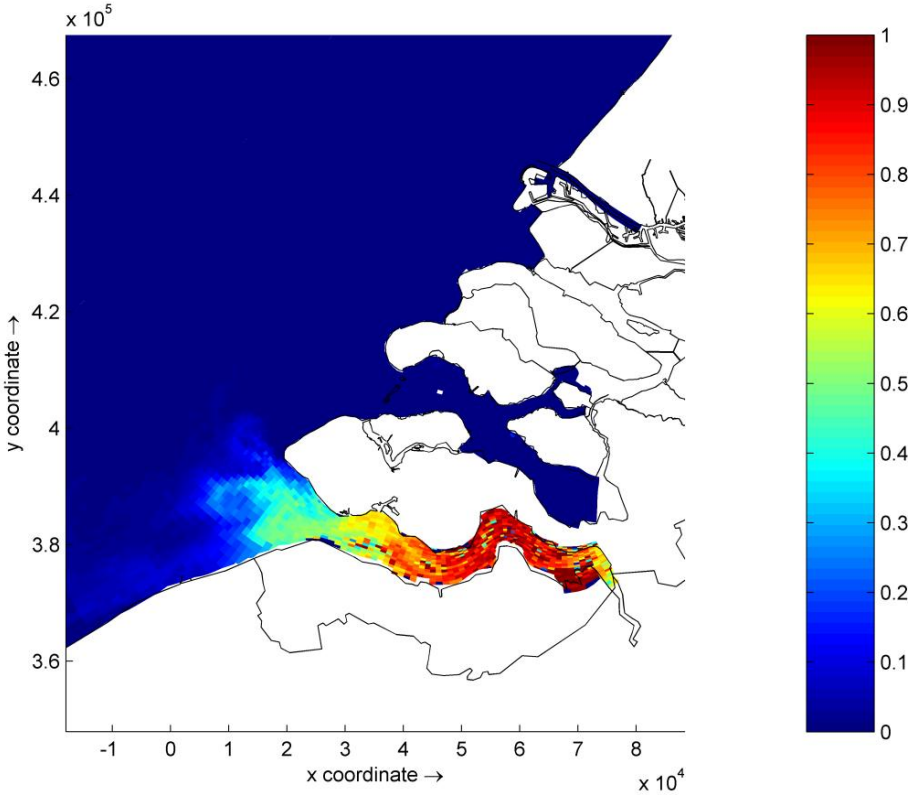

Figure 7. Final concentration ($N\,m^{-3}$) relative to an assumed initial concentration of 1.0 ($N\,m^{-3}$) for the Western Scheldt July simulation.

OSD
11, 1561–1611, 2014

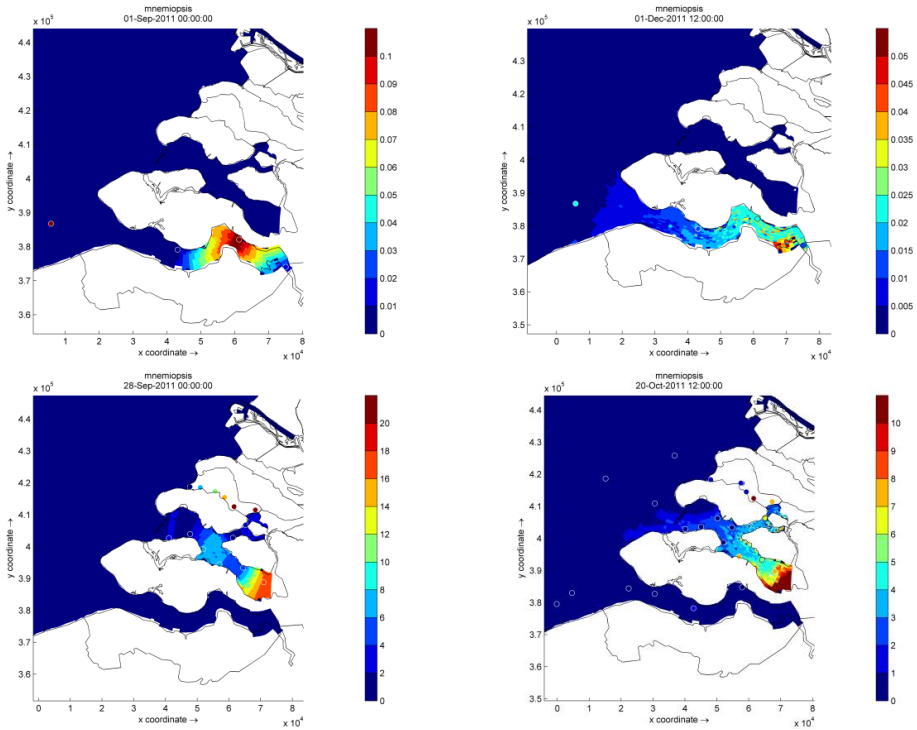

Figure 8. Observed density *M. leidyi* (individuals m^{-3}), realistic runs for 2011. (**a** and **c**): initial density based on field observations (circles) for Western and Eastern Scheldt, respectively. (**b** and **d**): final simulated density and field observations (circles) for Western and Eastern Scheldt, respectively.

OSD
11, 1561–1611, 2014

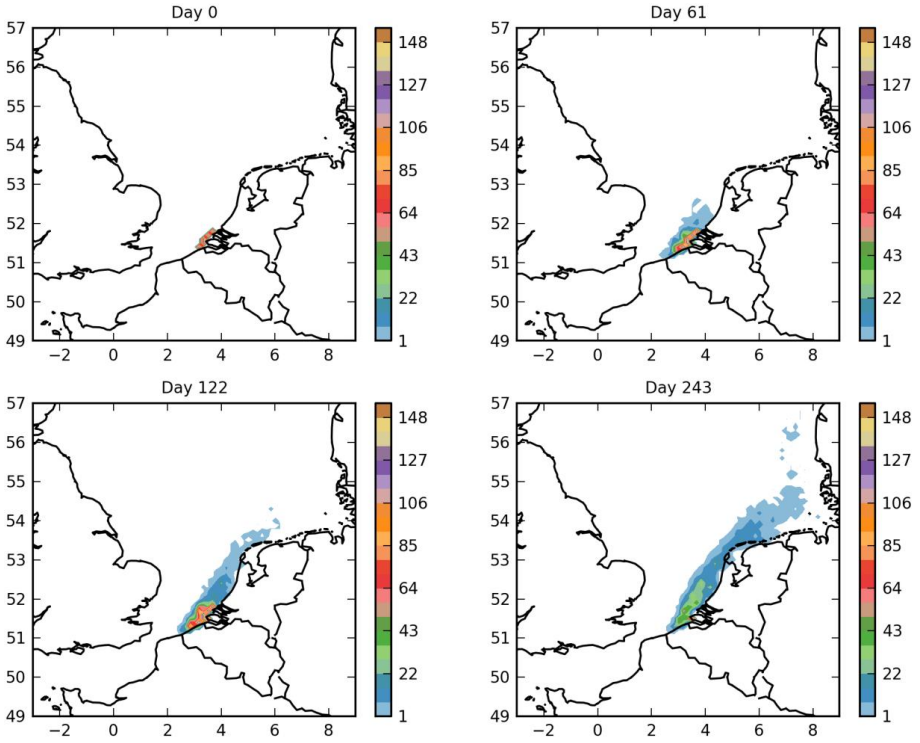

Figure 9. Density of particles on the model grid (number of particles per grid cell). **(a)** on day 1 of the simulation (1 June 2008); **(b)** on day 61 (31 July 2008); **(c)** on day 121 (29 September 2008); **(d)** on day 240 (25 January 2009).

OSD
11, 1561–1611, 2014

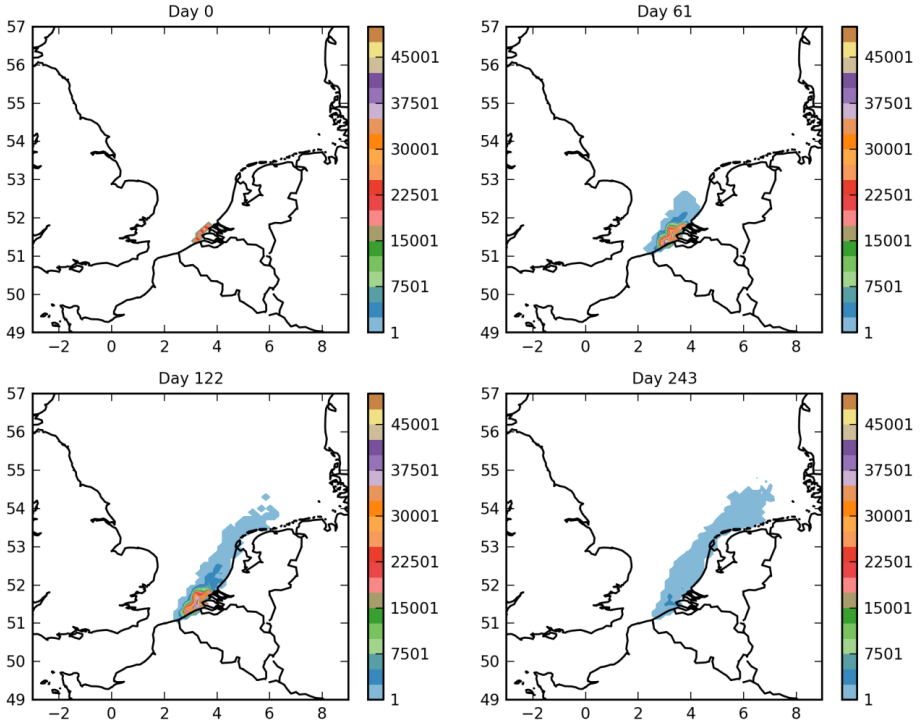

Figure 10. Density of simulated *M. leidyi* individuals on the model grid (number of individuals per grid cell). **(a)** on day 1 of the simulation (1 June 2008); **(b)** on day 61 (31 July 2008); **(c)** on day 121 (29 September 2008); **(d)** on day 240 (25 January 2009).

OSD
11, 1561–1611, 2014

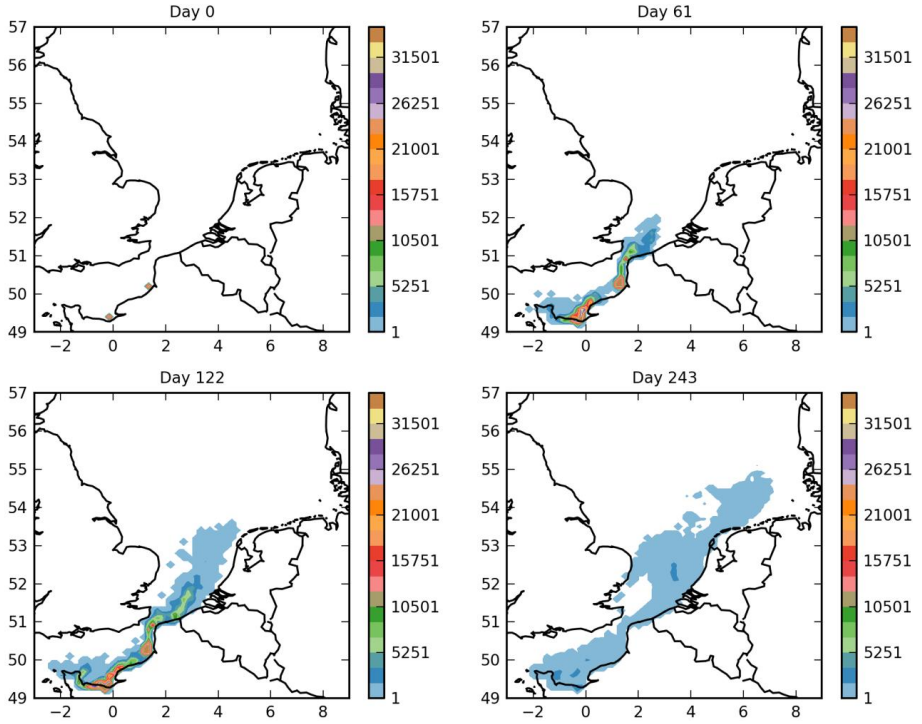

Figure 11. Density of simulated *M. leidyi* individuals on the model grid (number of individuals per grid cell) for releases in the rivers Seine and Somme. **(a)** on day 1 of the simulation (1 June 2008); **(b)** on day 61 (31 July 2008); **(c)** on day 121 (29 September 2008); **(d)** on day 240 (25 January 2009).

OSD
11, 1561–1611, 2014

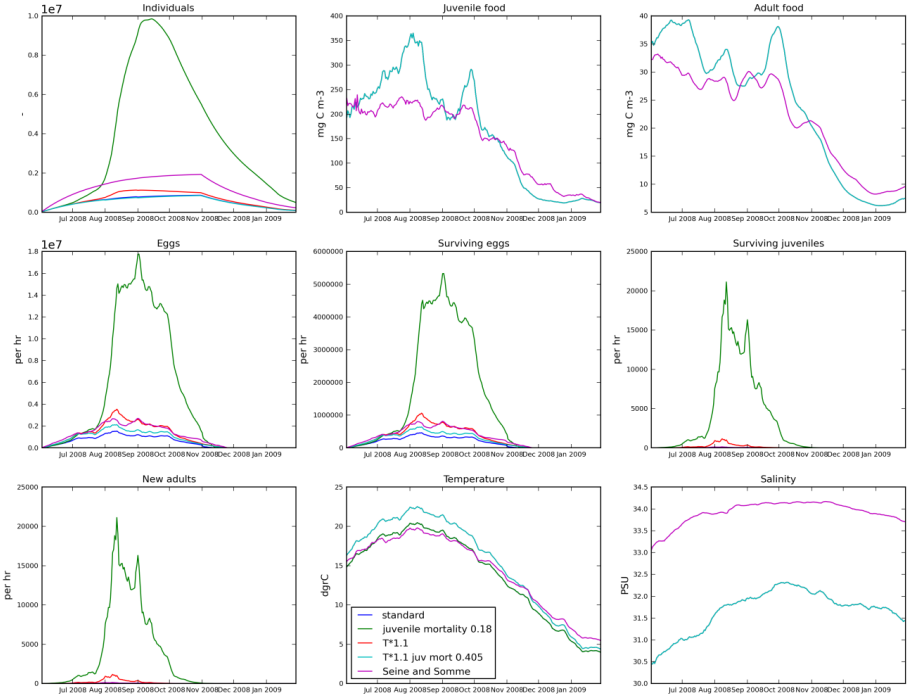

Figure 12. Cumulative results over all particles as a function of time for hindcast temperatures (dark blue), 1.1 times hindcast temperatures (red), two-thirds of juvenile mortality (green), combined 1.1 times hindcast temperatures and four-thirds of juvenile mortality (light blue), and release from the Seine and Somme (magenta). **(a)** Simulated number of *M. leidyi* individuals; **(b)** average juvenile food concentration available to particles [mg C m^{-3}]; **(c)** average adult food concentration available to particles [mg C m^{-3}]; **(d)** total number of eggs released per hour; **(e)** total number of surviving eggs per hour; **(f)** total number of surviving juveniles per hour; **(g)** total number of adults added to the population through reproduction per hour; **(h)** average temperature experienced by the particles; **(i)** average salinity experienced by the particles.

OSD
11, 1561–1611, 2014

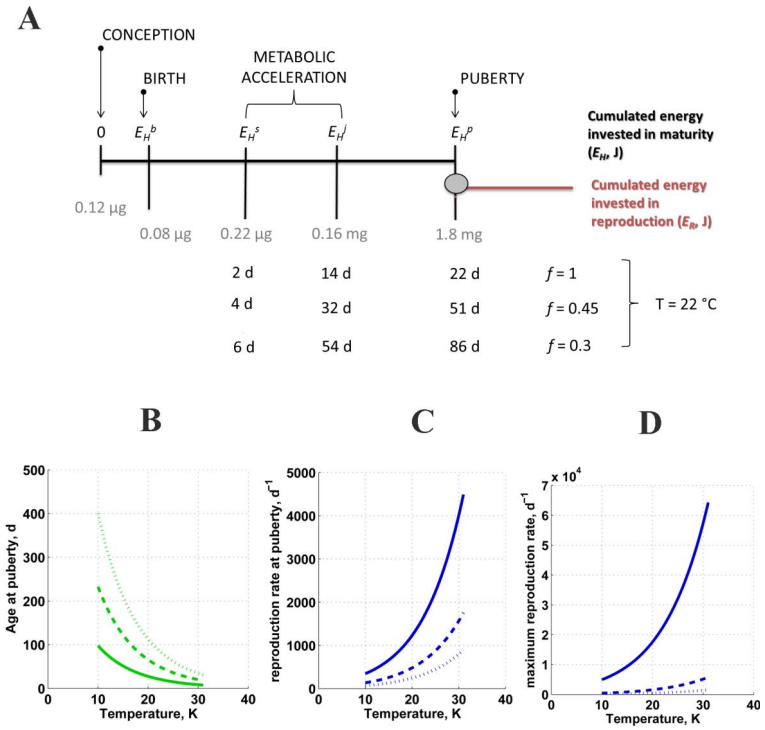

Figure 13. Results of DEB model simulations – **(A)** grey: carbon mass at stage transitions at f = 1. Below are presented the ages at each stage transition for three different ingestion levels ranging from1 to 0.3. **(B)** Age at puberty as function of temperature. **(C–B)** Reproduction rate at puberty and at ultimate mass and respectively as function of temperature. **(A–C)** Simulations are for three ingestion levels: f = 1 (solid line), f = 0.45 (dashed line) and f = 0.3 (dotted line).

OSD
11, 1561–1611, 2014

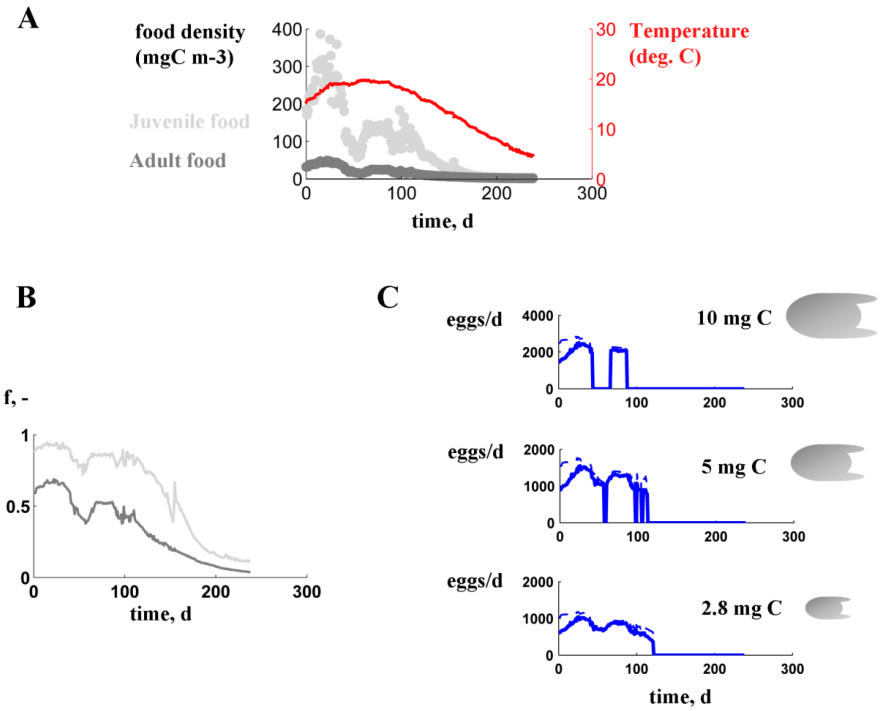

Figure 14. (A) Adult and juvenile food density in combination with temperature experienced by one particle. **(B)** Scaled functional response f (–) assuming $\{\dot{F}_m\} = 4\,\mathrm{L\,d^{-1}\,cm^{-2}}$ for juveniles (light grey) and adult (dark grey). **(C)** We simulate the combined effects of temperature and ingestion level on the daily reproduction rates of a 10, 5 and 2.8 mg C individual. The dashed lines assume a constant temperature of 20 °C. For each size class there is a minimum ingestion level for which maintenance can no longer be paid. We assumed that there was no reproduction when f decreased underneath that minimum, see text.

OSD
11, 1561–1611, 2014